31

Linearized Prebuckling: Examples and Limitations

TABLE OF CONTENTS

§31.1. Introduction

This Chapter present several examples of LPB analysis using the `PFabule` program described in Chapter 30. Both symbolic and numerical computations are illustrates. The examples are is followed by a more detailed study of the assumptions behind LPB, which were stated informally in Chapter 29. Practical limitations that emanate from these assumptions are then discussed, with emphasis on types of structures that are suitable for LPB.

§31.2. Rigid Column Examples

The examples here pertain to rigid columns where the flexibilities are lumpled into resisting springs. These are elegantly treated by the equilibrium method, which is not bothered by infinite member rigidities. The FEM/DSM analysis via `PFabule` is more complicated and requires special tools such as master-slave transformation to reduce freedoms, but is presented here to show that it can be done.

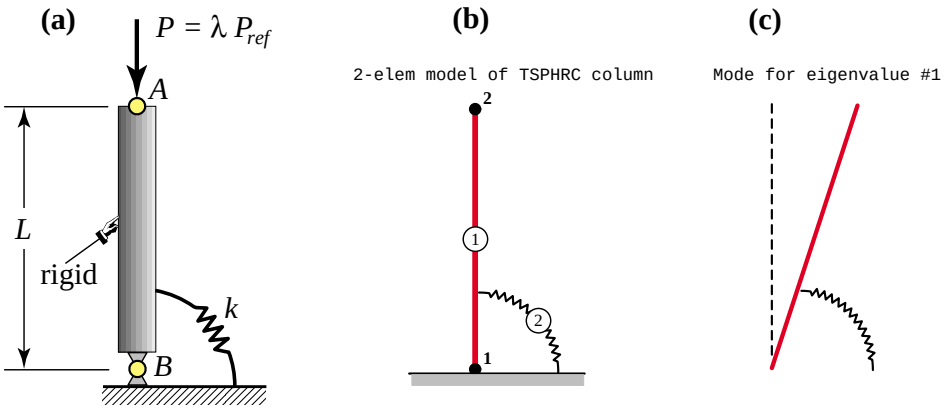

FIGURE 31.1. Buckling of Torsional Spring Propped Hinged Rigid Column (TSPHRC) using `PFabule`: (a) column; (b) 2-element FEM discretization with `PFabule`, and (c) buckling mode.

§31.2.1. TSPHRC Column

We retake the Torsional Spring Propped Hinged Rigid Column, or TSPHRC, which was analyzed in §28.5.1. The problem is shown in Figure 31.1(a). The FEM model has two elements: a beam column and a torsional string, as shown in Figure 31.1(b). The prebuckling part of the analysis can be skipped because the initial stress in the column is known to be $-P/A$ from statics.

The `PFabule` script for symbolic analysis is shown in Figure 31.2. The only nontrivial part is the master-slave freedom transformation that converts the elastic beam-column into a rigid one. This proceeds as follows. After imposing the bottom hinge condition and the inextensibility constrain, three DOF remain: θ_1, u_{X2}, and θ_2. Taking θ_1 as master, and u_{X2} and θ_2 as slaves, the rigidity condition is enforced by the displacement transformation:

$$\begin{bmatrix} \theta_1 \\ u_{X2} \\ \theta_2 \end{bmatrix} = \begin{bmatrix} 1 \\ -L \\ 1 \end{bmatrix} \theta_1. \tag{31.1}$$

```
ClearAll[L,Em,A,Izz,kT,P,λ];  data={L->1}; P=1;
NodeCoord={{0,0},{0,L}}; ElemType={"Beam","SpringT"};
numele=Length[ElemType]; numnod=Length[NodeCoord];
ElemNodes={{1,2},{1}}; ElemMaterial={Em}; ProcOptions={False,L>0};
ElemFabrication={{A,Izz},{kT,{1,2},L/5}};
numele=Length[ElemType]; numnod=Length[NodeCoord];
NodeTags={{1,1,0},{0,1,0}}; NodeValues={{0,0,0},{0,0,0}};
ElemIniStress={-P/A,0}; Tdof=Transpose[{{1,-L,1}}];
tcinfo={{4,"Red"},{2,"Blue"},{1,"Black"}}; ainfo={0,0.8,1.1};
einfo={0.06}; ninfo={0.03,2.,1.6}; backgr="YellowBG"; imgsiz=200;
PFabulePlotFEMModel[NodeCoord/.data,ElemType,ElemNodes,{},tcinfo,ainfo,
   einfo,ninfo,False,backgr,imgsiz,"2-elem model of TSPHRC Column"];
{KMred,KGred}=PFabuleEigenMatrices[NodeCoord,ElemType,ElemNodes,
ElemMaterial,ElemFabrication,ElemIniStress,NodeTags,Tdof,ProcOptions];
Print["KMred=",KMred//MatrixForm,"  KGred=",KGred//MatrixForm];
{λv,V}=PFabuleEigenSolution[KMred,KGred,NodeTags,NodeValues,Tdof,
True,False,ProcOptions]; Print["λv=",λv];  Print["V=",V//MatrixForm];
tcinfo={{3,"Red"},{2,"Blue"},{1,"Black"},{1.5,"Black"}}; amp=-1/3;
For [i=1,i<=Length[V],i++,vi=N[V[[i]]/.data];
    PFabulePlotDeformedShape[NodeCoord/.data,ElemType,ElemNodes,{},vi,amp,1,
    tcinfo,ainfo,False,backgr,imgsiz,"Mode for eigenvalue #"<>ToString[i]]];
```

FIGURE 31.2. `PFabule` script to analyze the Torsional Spring Propped Hinged Rigid Column (TSPHRC).

The 3×1 transformation matrix in (31.1) is called `Tdof` in the script. Upon performaing a congruential transformation on both $\mathbf{K}_{Mred}$ and $\mathbf{K}_{Gred}$ the eigensystem reduces to one DOF:

$$[\, k_T \,]\theta_1 = \lambda \, [\, 1/L \,]\theta_1. \tag{31.2}$$

This gives the only eigenvalue

$$\lambda_1 = K_T/L, \tag{31.3}$$

which agrees with that obtained with the equilibrium method in §28.5.1. The associated eigenvector is $\theta_1 = const$, which is depicted in Figure 31.1(c).

§31.3. Elastic Column Examples

We proceed next to elastic columns. These are modeled effectively by FEM — rigidity constraints do not get in the way. All examples are done symbolically, which necessarily restricts the number of elements and nodes to a very small number. The payoff is that dependence on free parameters can be explicitly obtained. That physics gets obscured when doing purely numerical work.

§31.3.1. Euler Column

The pinned-pinned, axially-loaded prismatic column pictured in Figure 31.3(a) will be called the *Euler column* for brevity. Its analytical solution for LPB critical loads is well known and often used as the first textbook example for that topic. Figure 31.3(b–d) depicts a FEM model with two beam column elements and three nodes.

Even for this simple problem, the aplication of boundary conditions (BC) requires some care. Figure 31.3(b) shows the BC for the initial-stress prebuckling analysis, in which the column remains vertical: $u_{X1} = u_{Y1} = u_{X2} = u_{X3} = 0$. It is important to let u_{Y2} and u_{Y3} be free, so the column is able to shorten under axial compression to develop axial stress $\sigma_{YY} = -P/A_0$. On the other

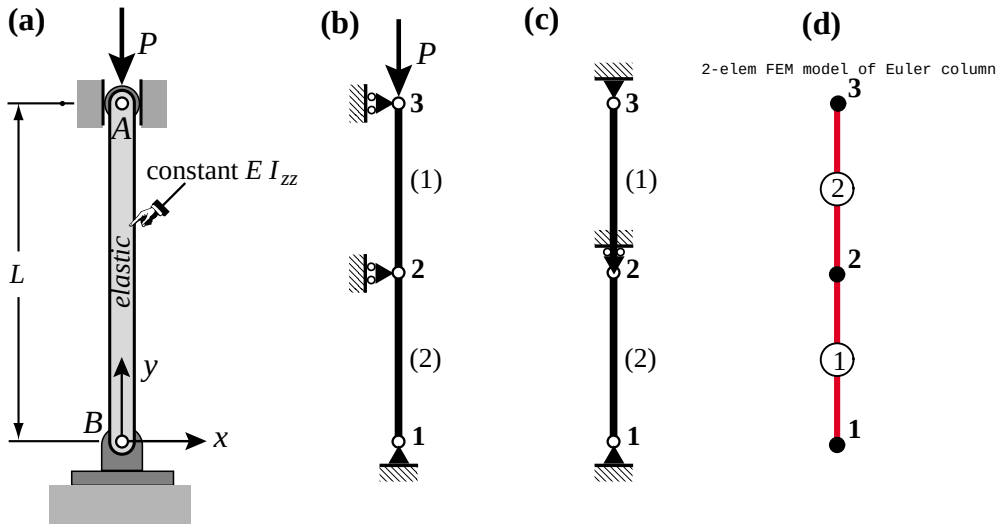

FIGURE 31.3. Buckling of Euler Column using a 2-element FEM discretization: (a) Euler Column sketch; (b) FEM model showing the BC appropriate for prebuckling analysis (axial shortening must be allowed); (c) same model showing BC used for LPB analysis; (d) `PFabule` model plot with yellow background removed.

hand Figure 31.3(c) shows BC for the buckling analysis. In accordance with the LPB assumptions we now "freeze" the axial motion by setting $u_{Y2} = u_{Y3} = 0$; however u_{X2} must be released since buckling necessarily involves lateral motions.

Figure 31.4 lists the `PFabule` script that sets up and analyzes the FEM model. Note that the initial stress prebuckling analysis is skipped since from static we know that the initial stress is $-P/A$ in both elements. Consequently only one BC set — that corresponding to Figure 31.3(c) — is used in the script. This leaves 4 active DOF: θ_1, u_{X2}, θ_2 and θ_3. The output from the analysis, except for the FEM model plot, which was moved to Figure 31.3(d), is collected in Figure 31.5. To save space, output cells have been captured and rearranged to compose that figure.

The analysis is fully symbolic. Except for the $E\,I_{zz}/L^2$ factor, the four computed eigenvalues are $\lambda_i = \gamma_i\, E\, I_{zz}/L^2$, where $gamma_i$ is dimensionless. The analysis gives

$$\gamma_1, \ldots \gamma_4 = \left\{240,\, 48,\, \frac{240}{13-2\sqrt{31}},\, \frac{240}{13+2\sqrt{31}}\right\} = \{\,240.,\, 48.,\, 128.723,\, 9.94385\,\}. \qquad (31.4)$$

The returned eigenvalues are unordered, which is typical of a symbolic analysis. The corresponding eigenvector (mode shape) plots are shown in Figure 31.5. #1 and #3 are (A) modes while #2 and #4 are (S) modes. Clearly λ_4 is a good approximation to the lowest critical load factor, which is $\gamma_{cr} = \pi^2 = 9.86960$, with error of 0.075%. The error grows for the other eigenvalues when compared to $4\pi^2 \approx 40$, $9\pi^2 \approx 90$ and $16\pi^2 \approx 160$, but only the lowest one has design significance.

The script of Figure 31.4 is parameterized by the number of elements `numele` set in the first code line. Symbolic analysis works for 1 through 3 elements. Beyond that the algebraic eigensolution fails (characteristic polynomail order becomes too high) and numerical analysis is required.

```
(* Define FEM model with numele (number of elements) as parameter *)

ClearAll[L,Em,A0,Izz,λ,P,numele]; numele=2; Le=L/numele; numnod=numele+1;
P=1; data={L->1,Em->1,A->1,Izz->1,P->1};
NodeCoord=Table[{0,Le*(n-1)},{n,numnod}]; pf=StandardForm;
PFabulePrintNodeCoord[NodeCoord,"Node coordinates:",{},{}];
ElemType=Table["Beam",{numele}]; ElemNodes=Table[{n,n+1},{n,numele}];
PFabulePrintElemTypeAndNodes[ElemType,ElemNodes,"Elem type and nodes:",{},{}];
ElemMaterial=Table[Em,{numele}]; ElemFabrication=Table[{A,Izz},{numele}];
PFabulePrintElemMatAndFab[ElemMaterial,ElemFabrication,"Elem mat and fab:",{},pf];
ElemIniStress=Table[-(P/A),{numele}];
PFabulePrintElemInitStress[ElemType,ElemIniStress,"Elem ini stresses:",{},pf];
NodeTags=Table[{0,1,0},{numnod}]; NodeTags[[1]]={1,1,0};
NodeTags[[numnod]]={1,1,0}; NodeValues=Table[{0,0,0},{numnod}];
PFabulePrintDOFActivity[NodeTags,NodeValues,"Node DOF activity:",{},{}];
numer=False; srule=L>0; ProcOptions={numer,srule}; Tdof={};
tcinfo={{4,"Red"},{2,"Blue"},{1,"Black"}}; ainfo={0,0.8,1.1};
einfo={0.06}; ninfo={0.03,2.,1.6}; backgr="YellowBG"; imgsiz=200;
PFabulePlotFEMModel[NodeCoord/.data,ElemType,ElemNodes,{},tcinfo,ainfo,
   einfo,ninfo,False,backgr,imgsiz,"2-elem FEM model of Euler Column"];

(*   Set up and solve LPB eigensystem *)

{KMred,KGred}=PFabuleEigenMatrices[NodeCoord,ElemType,ElemNodes,ElemMaterial,
        ElemFabrication,ElemIniStress,NodeTags,Tdof,ProcOptions];
facM=Em*Izz/L^3; facG=1/(L*60);
Print["KMred=",facM," ",Simplify[KMred/facM]//MatrixForm,
    "  KGred=",facG," ",Simplify[KGred/facG]//MatrixForm];
invKM=True; evonly=False; facλ=Em*Izz/L^2;
{λv,V}=PFabuleEigenSolution[KMred,KGred,NodeTags,NodeValues,
       Tdof,invKM,evonly,ProcOptions];
Print["λv=",facλ," ",Simplify[λv/facλ]," = ",facλ," ",N[Simplify[λv/facλ]]];

(* Plot buckling modes *)

Print["V=",N[V/.data]//MatrixForm]; amp=1/3; subs=15;
tcinfo={{3,"Red"},{2,"Blue"},{1,"Black"},{1.5,"Black"}};
For [i=1,i<=Length[V],i++,vi=N[V[[i]]/.data];
    PFabulePlotDeformedShape[NodeCoord/.data,ElemType,ElemNodes,{},vi,amp,subs,
    tcinfo,ainfo,False,backgr,imgsiz,"Mode for eigenvalue #"<>ToString[i]]];
```

FIGURE 31.4. Script to analyze the Euler Column with a two-element, three-node discretization. `PFabule`.

.

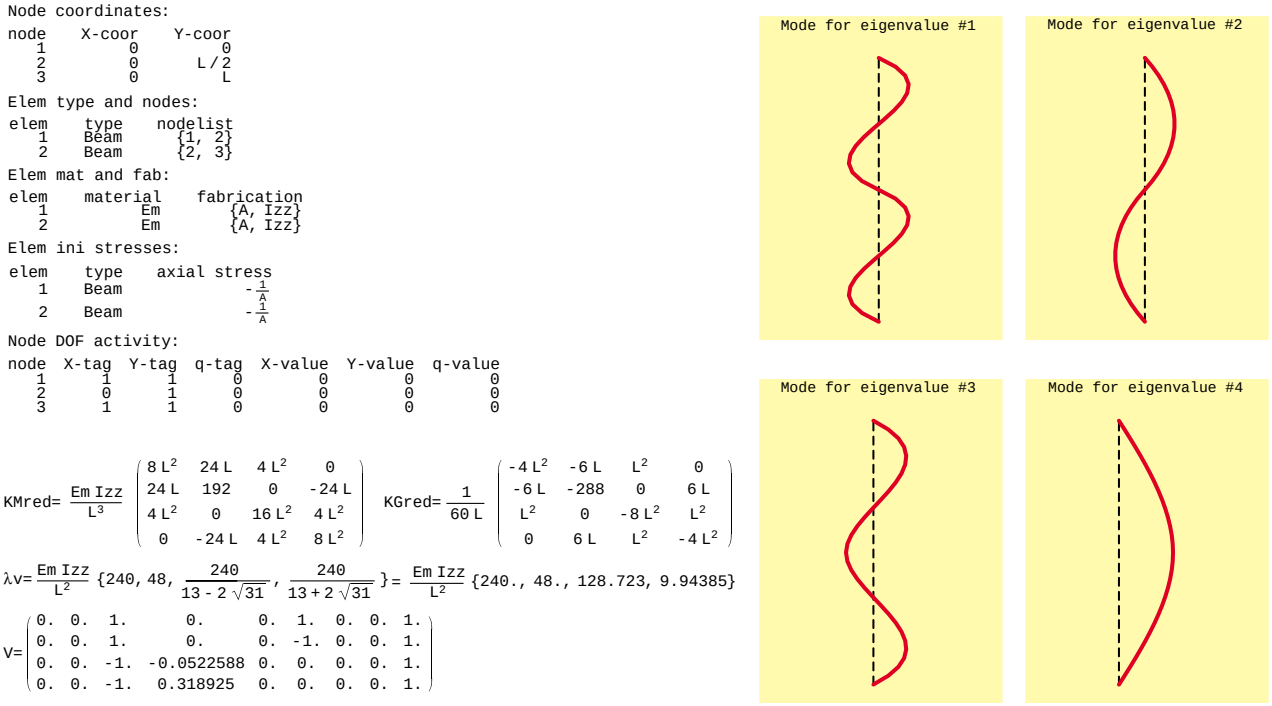

FIGURE 31.5. Results for Euler Column buckling using the `PFabule` script of previous figure.

§31.3.2. Euler Column with Midspan Spring

This is a variation of the problem of §31.3.1. A rectilinear spring of stiffness k_s is inserted at the column midspan, which is point C in Figure 31.6(a). (The column is continuous; there is no hinge at C.) For convenience in studying the effect of the spring on critical loads, its stiffness is expressed as

$$k_s = \beta \frac{E\, I_{zz}}{L^3}, \tag{31.5}$$

in which $\beta \geq 0$ is dimensionless. The spring has effect only if C moves laterally, as happens in symmetric (S) modes, but is inactive on antisymmetric (A) modes; see Figure 31.6(b). The `PFabule` script is not shown since it is a simple modification of that listed in Figure 31.4: only a rectilinear spring is inserted as element #3 as pictured in the model plot of Figure 31.6(c).

The general expression of the eigenvalues is $\lambda_i = \gamma_i E\, I_{zz}/L^2$, where γ_i is dimensionless. The `PFabule` result is

$$\gamma_1 = 240, \quad \gamma_2 = 48, \quad \gamma_3 = \frac{240(48+\beta)}{624+\beta-\Delta}, \quad \gamma_4 = \frac{240(48+\beta)}{624+\beta+\Delta}, \tag{31.6}$$

in which $\Delta = 624 + \beta + \sqrt{285696 - 912\beta + \beta^2}$. Modes #1 and #2 are antisymmetric and unaffected by the spring. Modes #3 and #4 are symmetric, and for these γ_i increases as β grows. That variation is diagrammed in Figure 31.7. Of some interest is the question: for which β do $\gamma_3 = 48$ and $\gamma_4(\beta)$ coalesce? A simple calculation shows that $\beta^* = 192$, a value marked in

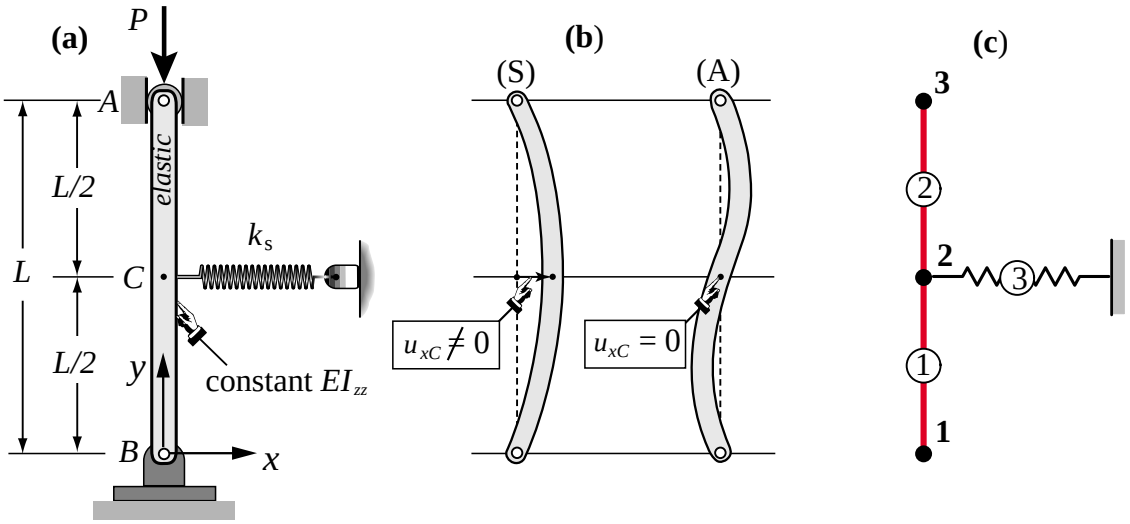

FIGURE 31.6. Euler Column with midspan spring: (a) problem defintion; (b) lowest symmetri9c (S) and antisymmtric (A) buckling modes; (c) `PFabule` model.

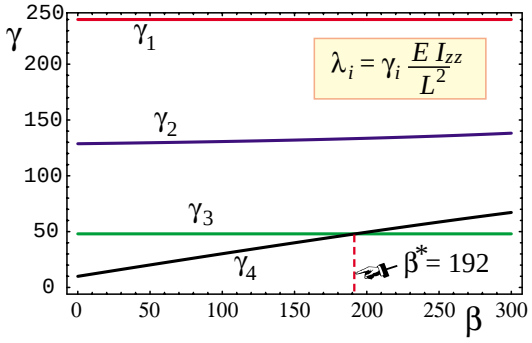

FIGURE 31.7. Euler Column with midspan spring: dependence of LPB eigenvalues on parameter β.

Figure 31.7. If β exceeds β^*, the column will fail antisymmetrically, and the critical load cannot be further raised by increasing the spring stiffness.

The exact characteristic equation for this problem, which can be obtained after about half hour of hand work, is

$$\frac{\lambda L\,(4\lambda^2 L^2 - \beta)\cos(\lambda L/2) + 2\beta \sin(\lambda L/2)}{4\lambda^2\, L^3} = 0. \tag{31.7}$$

This cannot be solved for λL in closed form if $\beta \neq 0$. But the coalescence of the two lowest buckling modes can be easily worked out and yields $\beta^*_{exact} = 16\pi^2 \approx 157.9$. Thus the FEM value $\beta^* = 192$ is about 21% in error. The discrepancy can be easily reduced by using more beam elements, but then numerical computation will be needed.

§31.4. Background for LPB Limitation Analysis

We now proceed to a critical analysis of the LPB limitations. As observed in **Notes and Bibliography**, this material cannot be (surprisingly) found anywhere else. Before discussing limitations, it is necessary to take a closer look at what happens near a bifurcation point.

§31.4.1. Analysis Assumptions

To state some of the LPB assumptions in mathematical plummage we introduce the concept of *state decomposition* at the bifurcation point to define homogeneous and particular solutions. This is done here primarily to introduce notation for **?**. The detailed mathematical analysis of this decomposition, when going beyond LPB to a general nonlinear response, is relegated to Chapter 33.

We restrict consideration to *isolated bifurcation points* of a *FEM discretized* system. Recall from Chapter 29 that an isolated bifurcation point at $\lambda_{cr} \equiv \lambda_B$ is characterized by a singular tangent stiffness at the equilibrium configuration,

$$\mathbf{K}(\mathbf{u}_B, \lambda_B)\,\mathbf{z} = \mathbf{0}, \tag{31.8}$$

where the normalized null eigenvector (buckling mode) $\mathbf{z} \neq \mathbf{0}$, $\|\mathbf{z}\| = 1$ is orthogonal to the incremental load vector:

$$\mathbf{q}^T\mathbf{z} = \mathbf{z}^T\mathbf{q} = 0. \tag{31.9}$$

Assume that we have located an isolated bifurcation point B and computed the buckling mode $\mathbf{z}$. Our next task is to examine the behavior in the *neighborhood* of B. We shall be content with looking at the so-called *branching direction information*. This information characterizes the *tangents* to the two equilibrium branches that cross at B.

Consider the variation of the state vector $\mathbf{u}$ measured from its value $\mathbf{u}_B$ at buckling:

$$\Delta\mathbf{u} = \mathbf{u} - \mathbf{u}_B \tag{31.10}$$

Divide this increment by Δt, t being the pesudotime parameter introduced in Chapter 3, and pass to the limit:

$$\dot{\mathbf{u}} = \lim_{t\to 0} \frac{\Delta\mathbf{u}}{\Delta t}. \tag{31.11}$$

We set the pseudoclock so that $t = 0$ at B.

§31.4.2. State Decomposition at Bifurcation Point

The governing equation at B is the first-order rate incremental ODE $\mathbf{K}\,\dot{\mathbf{u}} = \mathbf{q}\,\dot{\lambda}$ shifted to B and linearized there. Thus $\mathbf{K} \equiv \mathbf{K}_B$ and $\mathbf{q} \equiv \mathbf{q}_B$, but subscript B is omitted below to reduce clutter. Decompose the right-hand side trivially as $(\mathbf{q} + \mathbf{0})\dot{\lambda}$. Accordingly split the solution as

$$\dot{\mathbf{u}} = (\mathbf{y} + \sigma\,\mathbf{z})\dot{\lambda}, \quad \text{subject to} \quad \mathbf{q}^T\mathbf{z} = 0. \tag{31.12}$$

Here σ is a nonzero scalar amplitude introduced for convenience. These two components solve the inhomogeneous and homogeneous equations:

$$\mathbf{K}\,\mathbf{y} = \mathbf{q}, \qquad \mathbf{K}\,\mathbf{z} = \mathbf{0}. \tag{31.13}$$

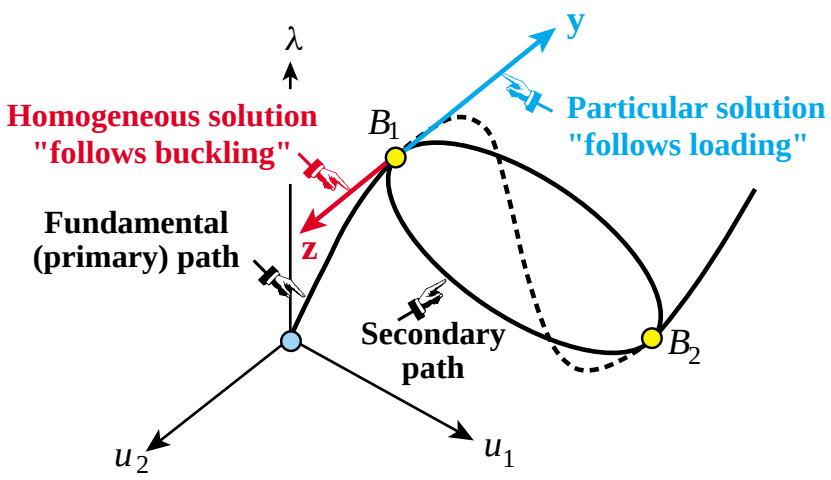

FIGURE 31.8. State decomposition at bifurcation point B: view in 3D control-state space. Vectors **y** and **z** are mutually orthogonal (proved in text). Together they define a plane in control-state space. All important physics happens in that plane, regardless of how many DOF the model has: 2 or a million. See next Figure.

while satifying the modified orthogonality conditions:

$$\mathbf{z}^T\mathbf{q} = 0 \;\Rightarrow\; \mathbf{z}^T\mathbf{K}\mathbf{y} = \mathbf{y}^T\mathbf{K}\mathbf{z} = 0. \tag{31.14}$$

Here we have used $\mathbf{K} = \mathbf{K}^T$. In accordance with classical ODE theory, we will label $\mathbf{y}\dot{\lambda}$ and $\mathbf{z}\dot{\lambda}$ the *particular* and *homogeneous* solutions, respectively, of the rate equation at B, occasionally dropping the $\dot{\lambda}$ factor. For the latter to nontrivially exist, $\mathbf{K}$ must be singular there, cf.(31.8).

The geometric interpretation of this decomposition on the control space of a system with two DOF is shown in Figure 31.8, which is largely patterned after Figure 5.2 The interpretation on the $\mathbf{y}$, $\mathbf{z}$ plane is shown in Figure 31.9. We emphasize that this picture is *universal*: all the important physics happens in this subspace, whether the system being analyzed has 2 or a million DOF.

§31.5. Consequences of LPB Assumptions

With the notation introduced in **?** we may now state precisely several key assumptions invoked in linearized prebuckling (LPB). (Those collected in item (II) have already been formally stated and used in previous Chapters)

(I) The external loading is conservative and proportional:

$$\mathbf{f} = \mathbf{q}_0 + \lambda\mathbf{q}. \tag{31.15}$$

and the structure is linearly elastic. In other words, the total residual equations are derivable from a potential energy function. As a consequence, $\mathbf{K}$ is symmetric: $\mathbf{K} = \mathbf{K}^T$.

(II) The displacements and displacement gradients prior to the critical state are negligible in the sense that (a) the *material stiffness matrix can be evaluated at the reference configuration*, and (b) the geometric stiffness is proportional to the control parameter λ:

$$\mathbf{K}_M \equiv \mathbf{K}_0, \qquad \mathbf{K}_G \equiv \lambda\mathbf{K}_1. \tag{31.16}$$

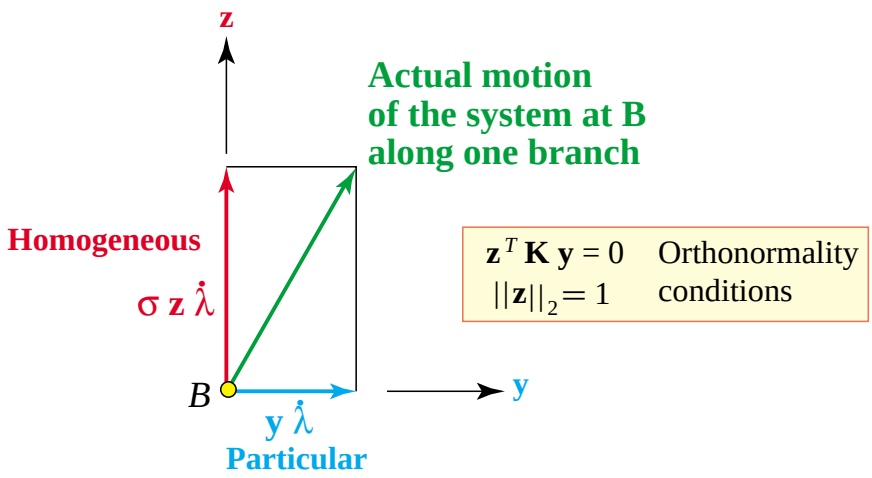

FIGURE 31.9. State decomposition at bifurcation point B, projected on the *y*-*z* plane.

Here $\mathbf{K}_0$ is the material matrix evaluated at the reference configuration, also called the *linear stiffness*, and $\mathbf{K}_1$ is the *reference geometric stiffness*. As discussed in §29.4, the singular stiffness test $\det \mathbf{K} = 0$ leads to the eigenproblem

$$(\mathbf{K}_0 + \lambda \mathbf{K}_1)\,\mathbf{z} = \mathbf{0}. \tag{31.17}$$

The λ that corresponds to the critical point under investigation will be called λ_{cr}. It is not assumed *a priori* that it is a bifurcation point.

(III) The particular solution $\mathbf{y}$ defined in §31.4.2 is obtained by solving

$$(\mathbf{K}_0 + \lambda_{cr}\,\mathbf{K}_1)\,\mathbf{y} = \mathbf{q} \tag{31.18}$$

under the constraint $\mathbf{y}^T\,\mathbf{K}\,\mathbf{z} = 0$. Observe that from assumption (I) $\mathbf{q}$ is constant.

We now prove that if these assumptions hold, all critical points determined from the LPB eigenproblem are *bifurcation* points, that is, $\mathbf{z}^T\mathbf{q}$ vanishes. To show that, premultiply both sides of (31.18) by $\mathbf{z}^T$:

$$\mathbf{z}^T\mathbf{q} = \mathbf{z}^T(\mathbf{K}_0 + \lambda_{cr}\,\mathbf{K}_1)\,\mathbf{y} = \mathbf{y}^T(\mathbf{K}_0 + \lambda_{cr}\mathbf{K}_1)\,\mathbf{z} = \mathbf{y}^T\,\mathbf{K}\,\mathbf{z} = 0, \tag{31.19}$$

in accordance with (31.14). Note that the matrix identity $\mathbf{z}^T\,\mathbf{K}\,\mathbf{y} = \mathbf{y}^T\,\mathbf{K}^T\,\mathbf{z} = \mathbf{y}^T\,\mathbf{K}\,\mathbf{z}$ holds because $\mathbf{K}_0$ and $\mathbf{K}_1$ are symmetric on account of the conservativeness assumption (I).

In Chapters 32–33 bifurcation points are further classified into asymmetric, stable-symmetric, unstable-symmetric, etc. It will be shown in Chapter 33 that LPB cannot reliably predict bifurcation points of *asymmetric* type, in which there is a *preferred* buckling direction. This is usually the case in shell buckling; for example circular tubes under compression can only buckle inwards.

§31.6. LPB Limitations

Linearized prebuckling (LPB) is used extensively in engineering design. Many standard books in structural stability only treat this technique. In its finite element version LPB is a feature available in many finite element programs. Exercising this feature has the advantages of avoiding a full

nonlinear analysis, which can be expensive and time-consuming. Given its practical importance, structure designers (and most especially aerospace designers) should be familiar with the range of applicability of LPB. The limitations are discussed next.

1. *Conservative loading*. LPB is a restricted form of the singular stiffness test (SST) criterion, also known as Euler's test; cf. §29.2. If the loads are not conservative, the dynamic criterion should be used, at least to check out whether a flutter condition may occur. If the dynamic criterion shows that stability is lost by divergence, one may regress to the SST.
2. *Static loading*. If the load is time-dependent, a dynamic criterion should be used.[1]
3. *Loss of stability must be by symmetric bifurcation*. If the first critical point is a limit point or asymmetric bifurcation,[2] LPB is not strictly applicable although occasionally it may provide a sufficiently good approximation. Lacking experimental confirmation or *a priori* knowledge, the only practical way to check whether the first critical point is symmetric bifurcation is to go through a full nonlinear analysis.
4. *Prebuckling deformations must be small*. This assumption fits well many engineering structures because of the nature of construction materials. The structures that best fit these assumptions are straight columns, frameworks and flat plates, as illustrated in Figure 31.10. Care must be exercised for arches, shells, very thin members, and for imperfection-sensitive structures in general.
5. *Elastic material behavior*. If the material is inelastic the structure is not internally conservative. Then the tangent stiffness depends on the prior deformation history, and the LPB eigenproblem loses meaning. The topic of inelastic buckling (in particular creep and plastic buckling) is a vast subject that falls outside the scope of this course.
6. *Applied loads should not depend nonlinearly on the displacements*. Such a dependence usually introduces nonconservative effects, thus voiding the conservative-loading assumptions. Even is the loads remain conservative, the reference geometric stiffness would depend on the load level, thus leading to a nonlinear eigenproblem.
7. *The effect of imperfections is negligible*. Some structures are highly *imperfection sensitive* in that the first critical load is strongly affected by the presence of imperfections. In such cases obviously LPB is of limited value or outright irrelevant.

§31.6.1. When LPB Works

The systems that best fit the LPB model are *symmetrically loaded structures* such as straight columns and in-plane-loaded plates (laminas) which are not excessively thin. See Figure 31.10. The lateral buckling of such structures occurs following very small deformations, as typified by the response sketch in Figure 31.11,

---

[1] If the load is periodic, this is known as *parametric stability* analysis in the literature.

[2] Symmetric bifurcation occurs when bucking in the $\mathbf{z}$ and $-\mathbf{z}$ directions is equally likely. Asymmetric bifurcation occurs when one of the directions is physically more likely; for example axially compressed cylinders buckle inwards. This classification of critical points is covered in more detail in Chapter 32–and following.

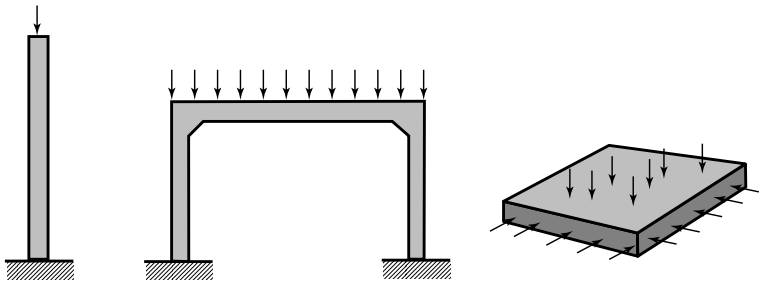

FIGURE 31.10. Structures that are adequately modeled by LPB assumptions.

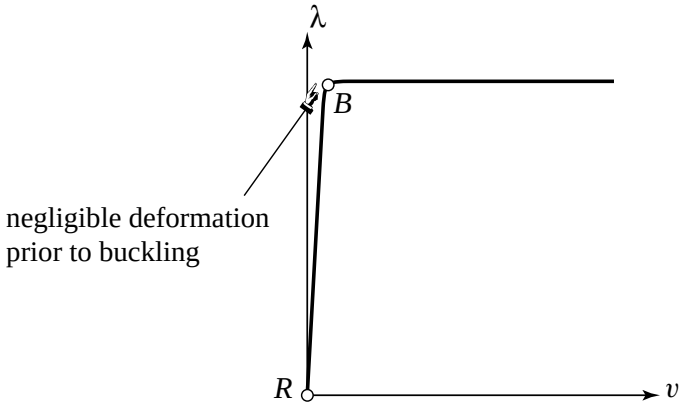

FIGURE 31.11. Type of response expected under LPB assumptions. (Branch intersection at B not shown for clarity)

§31.6.2. And When It Does Not

Two examples of structures that are not properly treated by the LPB model are shown in Figure 31.12. The LPB predictions are way off in both cases, but for different reasons.

Case (a) is an axially compressed cylindrical shell made up of almost flat panels joined by curved panels, forming like a "curved triangle" cross section seen in some combat helicopters as well as the Space Shuttle fuselage. There is a substantial redistribution of stresses due to changes on geometry. The structure eventually collapses at a limit point substantially over the predicted LPB load. The latter is therefore overly safe.

On the other hand, the axially compressed circular cylinder of case (b) is highly imperfection-sensitive structure that fails at a substantially lower load than that predicted by LPB. Consequently the LPB prediction is highly unsafe.

§31.6.3. Extending LPB Applicability

One way to broaden the application of the LPB model is to *update the reference configuration*[3] so that the prebuckling deformations are reduced. If this is done the control parameter λ is of course measured from the latest reference configuration and consequently becomes a true stage control

[3] As naturally done in the CR description, in which the deformational displacements are measured from a continuously varying configuration, and also in the Updated Lagrangian description.

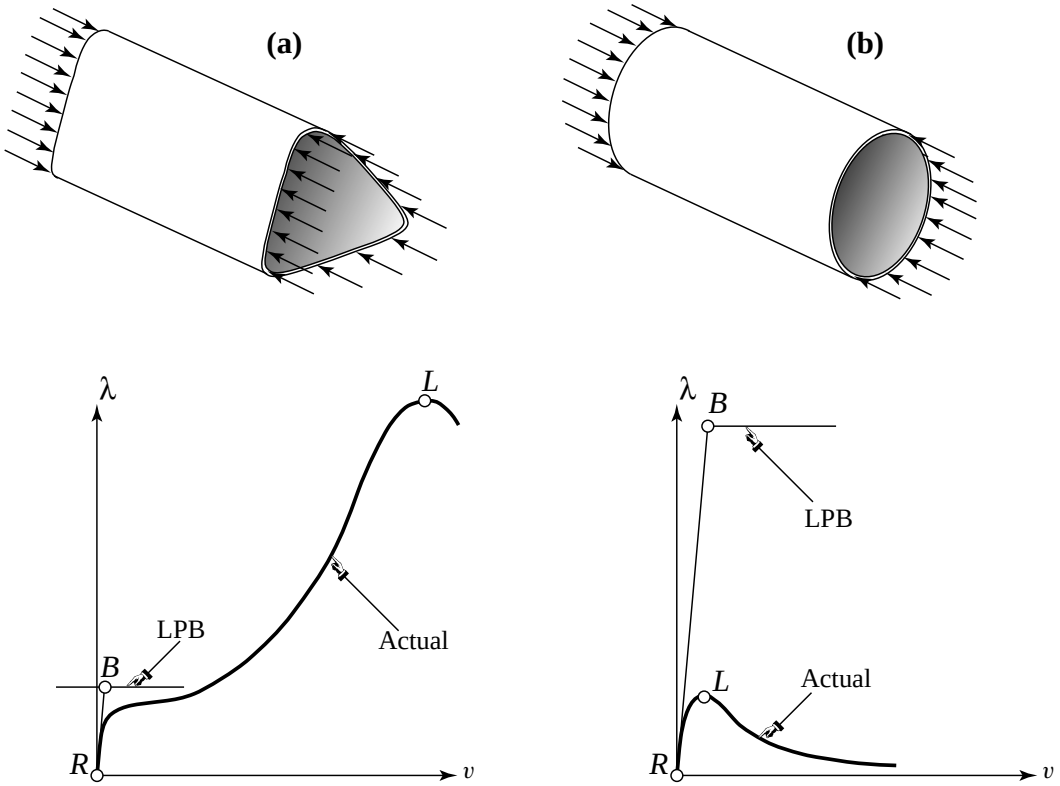

FIGURE 31.12. Structures that are poorly modeled by LPB assumptions.

parameter. Limitations on the conservativeness of applied loads and types of critical point, however, cannot be readily circumvented by this "staging" technique.

Notes and Bibliography

Significant attention has been placed on LPB because of its importance in structural design. Before computers it was the only practical method for assessing stability of complex structures.

There is a significant dearth of information as regards LPB limitations. In particular the analysis of **?**–§31.5 is surprisingly difficult to find in textbooks. The four tools used there are rate equations, linear ODE theory, orthogonality and (for conciseness) matrix algebra. Nothing fancy, only undergraduate math.

One would not expect to find this kind of study in Timoshenko and Gere [763], since their presentation focuses on details (exhaustively illustrated with examples) rather than principles, and none of the aforementioned math tools are ever used. Some more modern authors attempt perturbation analysis à la Koiter, e.g., [757], but the lack of matrix notation makes the stuff unreadable. Mathematical treatments such as [434] transport the unsuspecting reader to Banach spaces, to which Dante's "lasciate ogni speranza" dictum is pertinent.

Homework Exercises for Chapter 31

Linearized Prebuckling: Examples and Limitations

EXERCISE 31.1 [A:15] Find the particular solution $\mathbf{y}$ at the lowest bifurcation load of the two-bar example of Chapter 28.

EXERCISE 31.2 [A:15] Find the particular solution $\mathbf{y}$ at the symmetric and antisymmetric bifurcation loads of the one-element Euler column example of Exercise 24.4.

EXERCISE 31.3 [A:25] The first order residual rate equations is $\dot{\mathbf{r}} = \mathbf{0}$, where $\dot{\mathbf{r}}$ is given by

$$\dot{\mathbf{r}} = \mathbf{K}\dot{\mathbf{u}} - \mathbf{q}\dot{\lambda} = \mathbf{0}, \tag{E31.1}$$

(E28.1) holds at a bifurcation point where $\mathbf{K}$ and $\mathbf{q}$ are the tangent stiffness matrix and incremental load vector, respectively, at bifurcation. Decompose $\dot{\mathbf{u}} = (\mathbf{y} + \sigma\mathbf{z})\dot{\lambda}$, where $\mathbf{y}$ is the particular solution and $\mathbf{z} \neq \mathbf{0}$ the buckling mode normalized to length one. Show that the first-order differential equation system (E31.1) cannot give information on the "buckling mode amplitude" σ because one gets $\sigma = 0/0$. (Hint: premultiply that equation by an appropriate vector.)